



Effects of Island Topography on Storm Surge in Taiwan Strait during Typhoon Maria

Jie Yang¹; Chuan-yao Lin²; Haijiang Liu³; Linlin Li⁴; Tso-ren Wu⁵; Peitao Wang⁶; Benxia Li⁷; and Philip L.-F. Liu, Dist.M.ASCE⁸

Abstract: In July 2018, Super Typhoon Maria moved in the northwestward direction, passed by the northern tip of Taiwan Island, and severely impacted the coasts along Fujian and Zhejiang Provinces, China. In this paper, the storm surge and wind waves induced by Typhoon Maria are numerically simulated using a weather research and forecasting (WRF) model and the wind–surge–wave modeling suite [semi-implicit cross-scale hydroscience integrated system model (SCHISM)—wind wave model III (WWMIII)]. Numerical results are compared against available field measurements, including winds, atmospheric pressures, storm tides, and wave parameters. Using the model results, the significance of waves on modulating storm surges during Typhoon Maria is examined. Wind waves contribute significantly to surge heights in the Taiwan Strait and in nearshore waters. The models are then employed to conduct numerical experiments by reducing the topographic heights of Taiwan to 25% of their original values so as to investigate their effects on wind fields, surges, and currents. From these results, we observe that reduced topography weakens the wind intensity on the eastern side of the island while intensifying the wind on the other side of the island by up to 10 m/s, which is due to the terrain-induced blocking and channeling effects. The scenario with reduced topography also shows elevated surge heights on the right-hand side of typhoon landfalling coasts but slightly attenuated surge in the Taiwan Strait. Storm surge tends to increase the southwestwardly flux via the Taiwan Strait with maximum current velocities increased by approximately 0.5 m/s, compared with the case induced by astronomical tides only. The reduced island topography slightly weakens the southwestwardly current, decreasing maximum flux by approximately 16%, relative to the hindcast simulation using the original island topography. The results in this study indicate that the presence of island influences the propagation of surge wave with elevated surge height and storm-induced flux in the Taiwan Strait, this blocking effect weakens with reduced island topographic heights; meanwhile, the terrain-induced channeling effect, which alters the typhoon circulation and further impacts the surge pattern, is prone to forming in the case of high island topography. DOI: [10.1061/\(ASCE\)WW.1943-5460.0000619](https://doi.org/10.1061/(ASCE)WW.1943-5460.0000619). © 2020 American Society of Civil Engineers.

Author keywords: Typhoon Maria; Wind–island interaction; Taiwan Strait; Weather research and forecasting (WRF) model; Surge–wave interaction.

Introduction

Super Typhoon Maria was the first Category-5 (on the Saffir–Simpson scale) tropical cyclone (TC) occurring in the western North Pacific basin in 2018, and it was one of the strongest typhoons that affected Taiwan the last 2 years. In Fig. 1, the best track of Typhoon Maria and other characteristics are shown [CMA 2008; supported by China Meteorological Administration (CMA)]. Typhoon Maria underwent a rapid intensification after its generation near Guam on July 4, 2018 (20:00 UTC+8), and reached the super typhoon status on July 6, 2018 (05:00 UTC+8). Its high intensity lasted for more than 3 days with the 2-min maximum sustained wind above 52 m/s. During its

northwestwardly movement toward the Chinese coast, its track continuously shifted northly so that the final storm impacts on northern Taiwan were much reduced. Being affected by the subtropical high pressure, Typhoon Maria passed by the northern tip of Taiwan and moved toward the eastern coast of China with a forward speed as fast as approximately 30 km/h after July 8, 2018 (20:00 UTC+8). Although Typhoon Maria was downgraded to severe typhoon when it made its landfall in Ningde, Fujian Province on July 11, 2018 (09:10 UTC+8), with a maximum sustained wind of 48 m/s and a minimum central pressure of 960 hPa, it still severely affected the Fujian and Zhejiang coasts with storm surge heights of approximately 2.5 m and huge wave heights of up to 9 m.

¹Key Laboratory of Ministry of Education for Coastal Disaster and Protection, Hohai University, 1 Xikang Rd., Gulou District, Nanjing 210098, China (corresponding author). ORCID: <https://orcid.org/0000-0002-1083-1321>. Email: jie_yang@hhu.edu.cn

²Research Center for Environmental Changes, Academia Sinica, No. 128, Sec. 2, Academia Rd., Taipei 115201, Taiwan. Email: yao435@gate.sinica.edu.tw

³College of Civil Engineering and Architecture, Zhejiang Univ., 866 Yuhangtang Rd., Hangzhou 310058, China. Email: haijiangliu@zju.edu.cn

Note. This manuscript was submitted on May 12, 2020; approved on September 1, 2020; published online on November 30, 2020. Discussion period open until April 30, 2021; separate discussions must be submitted for individual papers. This paper is part of the *Journal of Waterway, Port, Coastal, and Ocean Engineering*, © ASCE, ISSN 0733-950X.

⁴Dept. of Earth Sciences and Engineering, Sun Yat-Sen Univ., 135 Xianggang Xi Rd., Guangzhou 510275, China. Email: lilinlin3@mail.sysu.edu.cn

⁵Graduate Institute of Hydrological and Oceanic Sciences, National Central Univ., No. 300, Zhongda Rd., Zhongli District, Taoyuan 32001, Taiwan. Email: tsoreun@ncu.edu.tw

⁶National Marine Environmental Forecasting Center (NMEFC), No. 8 Dahuisi Rd., Haidian District, Beijing 100081, China. Email: wpt@nmefc.cn

⁷National Marine Environmental Forecasting Center (NMEFC), No. 8 Dahuisi Rd., Haidian District, Beijing 100081, China. Email: lbx@nmefc.cn

⁸Dept. of Civil and Environmental Engineering, National Univ. of Singapore, Engineering Drive 2, Block E1A #07-03, Singapore 117576, Singapore. Email: Philip.Liu@nus.edu.sg

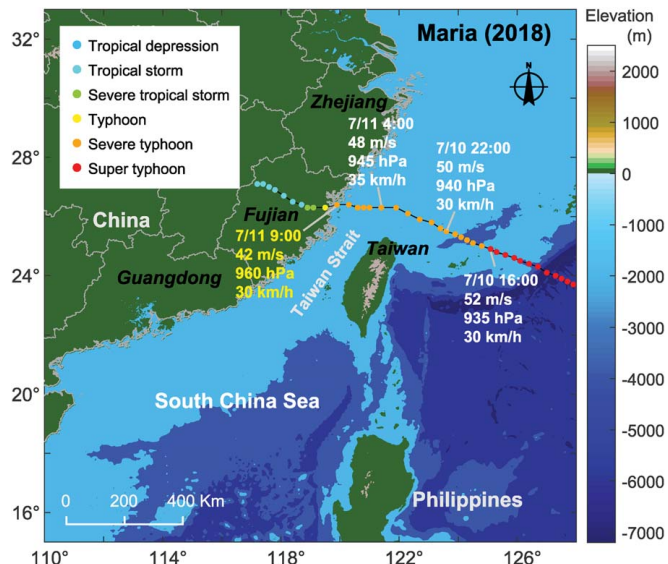


Fig. 1. (Color) Best track of Typhoon Maria from the Chinese typhoon weather website (time zone: UTC+8). (Data from CMA 2008.)

The existence of Taiwan Island can influence TCs moving across it or passing by, which results in the modulation of storm surges, waves, and currents in the vicinity of Taiwan. Taiwan suffers yearly 3–6 typhoons; the terrain of the Central Mountain Range (CMR), with an average elevation of 2,000 m and a peak close to 4,000 m, impacts typhoon motion such as track, intensity, structure, and associated rainfall (Huang et al. 2011). Due to great uncertainty in the prediction of storm track and intensity, a Maria-like TC moving toward northern Taiwan may alter its track to closer or farther locations when moving by the island and may be influenced by island topography to a different degree. Thus, Typhoon Maria can be a representative case study to examine typhoons moving by northern Taiwan and the associated surge and waves influenced by island topography. The effects of Taiwan on storm-induced processes have seldomly been examined in previous studies. Studies by Zhang et al. (2009, 2010) investigated the southward transport and intensified tide-surge interaction in the Taiwan Strait during typhoon events. Both realistic modeling of typhoon events and dynamic analysis from reduced terms in governing equations were employed in their studies. They concluded that the strong southward transport in the Taiwan Strait is majorly caused by storm-induced local wind stress and/or the along-strait water level gradient, while the tide-surge interaction is intensified mainly due to nonlinear bottom friction. Another study by Liu and Huang (2020) discussed how different factors, including waves and typhoon track, influence the surge height around the Taiwan coast, and they found that wave setup can contributes 6%–35% to the total storm surge. The aforementioned studies gained important knowledge on storm-induced processes and associated mechanisms under conditions of different typhoon tracks. Yet one limitation is that the influence of island topography on storm motions is not reflected in the upstream driving forces, which are applied to the surge-wave models.

The storm-induced surface wind shear and atmospheric pressure gradients are the primary forcing functions responsible for generating wind waves and storm surge. A variety of analytical and numerical models have been developed for resolving wind/pressure fields associated with storms (Emanuel and Rotunno 2011; Holland 1980; Vickery et al. 2009; Xie et al. 2006). The high-efficiency parametric vortex models are convenient; however, they cannot adequately

account for the interactions between a storm and land surfaces with increased bottom friction. The wind field associated with Typhoon Maria was deformed by the north–south elongated CMR on Taiwan, resulting in lower wind speed. Therefore, in this situation, full-scale physics-based dynamical climate models, such as the fifth-generation Penn State/National Center for Atmospheric Research mesoscale model (MM5) (Grell et al. 1994) and the weather research and forecasting (WRF) model (Skamarock et al. 2008), are expected to better reproduce the vertical profiles of storm wind and pressure fields. Although the Big Island (Hawaii) and Philippines topography have been studied for their effects on TC motion and change (Chambers and Li 2011; Tang and Chan 2014), the Taiwan Island has been a focus to investigate the topography's effects on track deflection and strength variation of typhoons, as well as rainfall asymmetry in previous studies. The most studied typhoons were those that made direct landfalls on the eastern coast of Taiwan, e.g., Typhoons Fanapi (2010), Morakot (2009) and Nari (2001) (Fang et al. 2011; Xie and Zhang 2012; Wang et al. 2013; Yang et al. 2008, 2011); several TCs moved close by Taiwan and affected the Taiwan Island have also been studied, e.g., the rapid intensification of Typhoon Meranti (2010) was promoted by topography-induced strong vertical motion (Xue and Li 2016). However, a nonidealized simulation of a typhoon moving close by the northern tip of Taiwan has rarely been examined interacting with high topography. Similarly, its further influence on storm surge in the vicinity of Taiwan has seldom been examined.

Previous studies of observations and numerical simulations support that both northward and southward deflections can occur for TCs approaching Taiwan. Northward deflections due to cyclonic circulation by the blocking effect are reported by Yeh and Elsberry (1993) and Wu (2001), while the channeling effect between the CMR and TC is believed to be the major factor resulting in the nearshore southward deflection of TCs (Jian and Wu 2008; Huang et al. 2011). Tang and Chan (2014, 2015, 2016a, b) systematically studied the effect of topography alone on TC tracks through idealized simulations; they identified the mechanisms of northward deflection for a TC approaching Taiwan. A pair of terrain-induced gyres in the low to mid-levels over the CMR on Taiwan would be advected cyclonically around the TC center, and the flow associated with the gyre pair would advect the TC core northeastward and lead to TC deflection northwardly. The extent of the upstream northward deflection mainly depends on the landfalling position, TC size, and steering flow strength. TCs approaching far south or north of Taiwan are also deflected by the remote topography effect, although the effect on the latter TCs is much weaker. The steep mesoscale topography of Taiwan often dictates the rainfall structure, which tends to increase the total amount significantly for TCs that make landfall or move close by (Fang et al. 2011; Xie and Zhang 2012) and further alter the TC motion (Wang et al. 2013). For example, Wang et al. (2013) reported that the asymmetric rainfall/latent heating induced by the blocking effect of CMR topography was the main reason that caused sudden and temporary speed reduction in track motion of Typhoon Fanapi (2010). Apart from various mechanisms that cause deflections of TCs approaching Taiwan, the evolution of TC intensity also depends on many factors and processes, such as vertical wind shear, moisture content of the storm environment, upper-level perturbations, sea surface temperature (SST) and the underlying oceanic mixed layer depth, latent heat release from TCs, and coastal surface conditions (Yang et al. 2008). In the present study, we intend to examine the change of typhoon track and intensity of Maria when interacting with island topography through numerical experiment with reduced topography heights of the Taiwan Island.

In the present study, a WRF model is used to generate the wind and atmospheric pressure field corresponding to Typhoon Maria. The two-way coupled SCHISM (tide–storm surge)–WWMIII (wave spectrum) model is then implemented to hindcast the dynamic wind–wave–storm surge processes during Typhoon Maria. The simulation modeling suite is first compared with measured wind, storm tide (sea surface elevation comprising the astronomical tidal elevation and the storm surge), and wave data in the region around Taiwan. The goals of this hindcasting simulation are to provide a comprehensive description of meteorological conditions and storm surge patterns associated with Typhoon Maria and to examine the dynamic characteristics of storm surges and ocean wind waves for a better understanding of the influence of island topography and wind waves on storm surges.

The contents in this paper are organized as follows: In the “Data and Methods” section, the domain of study, the input data, and model configurations for generating surface wind and pressure, surge, and waves are described. In the “Model Performance” section, the performance of the modeling suite is thoroughly compared with available measurements; in the “Additional Results and Discussions” section, we examine the main patterns of storm surges and wind waves and the effects of wind waves on surge heights. Additionally, the effects of Taiwan’s topography on the storm (wind/pressure) and the resulting impacts on waves, surges, and currents are discussed. Concluding remarks are provided in the final section.

Data and Methods

In this study, we use the data-assimilated WRF modeling system to hindcast the core structure and vertical profiles of Typhoon Maria. The simulated surface pressure and winds at 10-m height are used to drive a coupled surge–wave simulation model, which produces the storm surges and wind waves near Taiwan and along the coasts of Fujian and Zhejiang Provinces, China.

Surface Wind and Pressure Fields by WRF

In this study, the Advanced WRF modeling system (version 3.9.1.1) is used to generate the atmospheric fields (Skamarock et al. 2008). The meteorological initial and boundary conditions for WRF were obtained from the National Center for Environmental Prediction (NCEP) Global Data Assimilation System (GDAS) with $0.25^\circ \times 0.25^\circ$ analysis data sets at a 6-h interval. The time-varying SST was from the 0.5° NCEP real-time global sea surface temperature (RTG_SST) analysis dataset. The planetary boundary layer of the Yonsei University boundary layer scheme (Hong et al. 2006) is used with the revised MM5 Monin–Obukhov surface layer scheme (Jiménez et al. 2012) and the unified Noah land surface model (Tewari et al. 2004) over land. The single-moment five-class microphysics scheme (Hong et al. 2004), the updated Kain–Fritsch scheme (Kain 2004; Kain and Fritsch 1990) with a moisture-advection-based trigger function (Ma and Tan 2009), the rapid radiation transfer model for global circulation models (RRTMG) shortwave and longwave schemes (Iacono et al. 2008) are adopted in this study. The horizontal resolution is 3 km and the grid box has 921×593 points in the east–west and north–south directions, respectively. There are 45 vertical levels with the lowest level approximately 50 m above the surface.

To examine how the topography height of island affects the storm and surge pattern, two scenarios are included in the present study: the original height of the Taiwan Island as the *hindcast scenario* and a reduced height to 25% of Taiwan topography as the *reduced topography scenario*. The north–south elongated CMR on

Taiwan has mountains with altitudes close to or exceeding 3 km. Therefore, in the reduced topography scenario, the maximum topography height difference from the hindcast scenario is up to approximately 2 km.

Coupled Surge–Wave Modeling System

Several well-known numerical simulation packages for storm surge and wave spectrum, such as ADCIRC (tide–storm surge) + SWAN (wave spectrum) (Booij et al. 1999; Luettich et al. 1992), FVCOM + SWAVE (Chen et al. 2003), and SCHISM + WWMIII (Zhang et al. 2016), are available for hindcasting typhoon-induced storm surge. All of these models are based on the same physics. The major differences among them hinge on the numerical algorithms solving the model equations and the domain discretization. Chen et al. (2013) compared the stated three current–wave-coupled model suites in tidal simulation and dynamic responses to storms, in which SELFE (Zhang and Baptista 2008), the previous model of SCHISM (semi-implicit cross-scale hydroscience integrated system model; Zhang et al. 2016), was used in this comparison study. All three model suites are shown to have similar accuracy, and the major differences in model performance stem primarily from algorithms solving current–wave interaction, wetting–drying treatment, and bottom friction parameterization. As an upgrade of SELFE (Zhang and Baptista 2008), SCHISM has revamped key formulations, including a new implicit transport solver (TVD²), a new horizontal viscosity formulation, and a new higher-order scheme for momentum advection. It is now more robust and efficient in seamlessly simulating processes from deep ocean to shallow environments in estuaries and rivers (Zhang et al. 2016). The coupled SCHISM–WWMIII modeling system is capable of considering the contribution from wind waves via radiation stresses and accounting for wave refraction, shoaling, and diffraction induced by variable depths and currents and has been successfully employed to study several previous typhoon-induced surges (e.g., Fortunato et al. 2017; Krien et al. 2017; Liu et al. 2020). Most recently in our previous studies, a model for the South China Sea region using this coupled model suite has been established and used successfully to hindcast the storm surges associated with Typhoon Hato (2017) and Typhoon Mangkhut (2018), including the coastal flooding pattern in Macau (Li et al. 2018; Yang et al. 2019). Therefore, the SCHISM + WWMIII model suite was chosen to compute the storm tide resulting from the Typhoon Maria event.

SCHISM employs a highly efficient and accurate semi-implicit finite-element/finite-volume method in conjunction with an Eulerian–Lagrangian algorithm to solve the hydrostatic form of the Navier–Stokes equations on the unstructured grid. The 2D depth-integrated (2DH) barotropic mode of SCHISM is utilized in this study. The wind drag coefficient on the water surface is calculated using the formula by Pond and Pickard (1983) and has a linear relationship with the 10-m height wind and has a capped value of 3.76×10^{-3} . The bottom drag is modeled by a depth-dependent quadratic friction law, with a drag coefficient described by Manning’s *n* value. The spectral wave model, wind wave model III (WWMIII) (Hsu et al. 2005; Roland et al. 2009), is embedded into SCHISM at the source code level. The WWMIII uses triangular elements in the geographical space to solve the wave action equation (WAE) and utilizes the same suite of unstructured meshes as SCHISM. In this spectral wave model, the surface wind, wave–wave interactions, white-capping, bottom friction, and depth-limited wave breaking have been considered as source terms of energy transfer or dissipation.

Computational Domain and Configurations

An unstructured mesh has been created for surge–wave coupling simulation in the computational domain covering the Yellow Sea, the East China Sea, and the South China Sea (Fig. 2). The mesh has a variable resolution, ranging from a coarser resolution of 25 km along the southeast open sea boundary, to a resolution of 2.5 km over the continental shelf, and to the finest resolution of approximately 700 m along a certain portion of coasts. The mesh has a total of 520,256 vertices and 1,017,501 elements. The overlaid bathymetry from the 30 arc-second General Bathymetric Chart of the Ocean data (GEBCO) is mapped onto mesh nodes, and higher resolution datasets from different sources are used for the areas of interest in this study, including 48 nautical charts with scales ranging from 1:5,000 to 1:750,000 from the Navigation Guarantee Department of Chinese Navy Head Quarters for the coasts along Zhejiang, Fujian, and Guangdong Provinces; 500-m resolution digital bathymetry data in the vicinity of Taiwan; 500-m resolution digital bathymetry data in the vicinity of Hong Kong from the Hydrographic Office, Marine Department. All utilized datasets are adjusted to the mean sea level (MSL).

In the present work, the spectral wave model WWMIII is applied with 35 frequency components with exponential distribution (i.e., $f_{n+1} = 1.1 \cdot f_n$ and $f_0 = 0.039$ Hz, $n = 0, 1, 2, \dots, 34$) and 24 direction bins with 15° resolution. Apart from driving forces of the 10-m height wind and surface pressure fields generated by the WRF model, time series of tidal elevation extracted from the TPXO8-atlas release of the OSU TOPEX/Poseidon Global Inverse Solution model (Egbert and Erofeeva 2002) and the global numerical solutions of a 3-h wave spectrum from WAVEWATCHIII (Tolman et al. 2002, 2005) are applied to the open ocean boundaries. The water surface elevation and current velocity in SCHISM are updated every 5 s and are passed to WWMIII every 600 s; the wave effects on storm surge are fed back via the calculated wave radiation stresses.

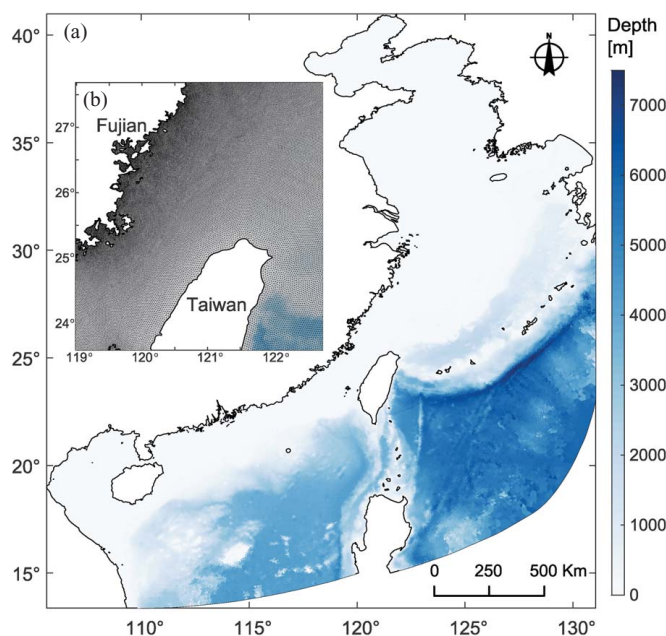


Fig. 2. (Color) (a) Computational domain for the SCHISM–WWMIII model package, with the bathymetry map; and (b) the close-up showing the mesh near coasts of Fujian Province and Taiwan.

Statistical Metrics for Assessing Model Performance

To quantify the skills of the WRF model and the tide–surge–wave-coupled model in predicting winds, atmospheric pressures, tides, storm tides, and wave parameters, three statistical metrics, including correlation coefficient R , root-mean-square error (RMSE), and bias, were used in this study. The correlation coefficient examines the overall model performance by calculating the agreement between model results and measurements, and a perfect agreement yields a value of 1. The RMSE and bias assess the absolute error between the modeled results and the measurements. An ideal value of zero indicates a perfect fit between the model results and the measurements for both RMSE and bias. Moreover, positive and negative values of bias indicate an overestimation and underestimation of model predication, respectively. These three metrics are defined as follows:

$$R(X, Y) = \frac{\sum_{i=1}^N (y_i - \bar{y})(x_i - \bar{x})}{\sqrt{\sum_{i=1}^N (y_i - \bar{y})^2} \sqrt{\sum_{i=1}^N (x_i - \bar{x})^2}} \quad (1)$$

$$\text{RMSE}(X, Y) = \sqrt{\frac{1}{N} \sum_{i=1}^N (y_i - x_i)^2} \quad (2)$$

$$\text{Bias}(X, Y) = \frac{1}{N} \sum_{i=1}^N (y_i - x_i) \quad (3)$$

where X and Y = measurement samples and model result samples, respectively; N = number of samples; and \bar{x} and \bar{y} = average values of the measured samples and the modeled samples, respectively.

Model Performance

The performance of the wind–surge–wave modeling suite is evaluated by comparing the measured meteorological conditions, astronomical tides, storm tides, and wind waves with the simulated results. The data for atmospheric pressures and winds are obtained from NOAA National Centers for Environmental Information. The time series of astronomical tides are retrieved from the University of Hawaii Sea Level Center (UHSLC). The measurements of total water levels and wave parameters during Typhoon Maria are collected from tidal gauges and wave buoys maintained by the State Oceanic Administration (SOA) of China and the Central Weather Bureau (CWB) in Taiwan, respectively. Additionally, the wave heights from the Jason-3 altimeter data (National Environmental Satellite Data and Information Service, 2018) are also used to evaluate the model skill. An overall view of station locations involved in this study is shown in Fig. 3.

Astronomical Tide

Tide-induced variations of sea surface elevation should be accurately reproduced by the hydrodynamic model prior to its application to the simulation of storm tides. Therefore, we have compared the model results with the water level variations for a two-month period starting from January 1, 2015, at five selected tidal gauges (see Stations 6–10 in Fig. 3 for detailed locations). Simulation results shown in Fig. 4 indicate that the tidal water levels can be reproduced with reasonable agreement in the South China Sea and the East China Sea. The values of RMSE are smaller than 0.01 m, except at the Quarry Bay station, where the tidal amplitude was slightly overestimated. This may have been caused by the

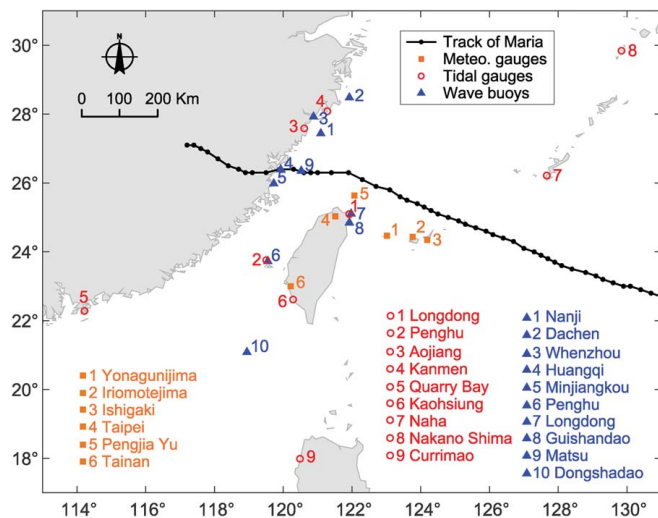


Fig. 3. (Color) Station locations of meteorological gauges, tidal gauges, and wave buoys. The best track data are from the Chinese typhoon weather website. (Data from CMA 2008.)

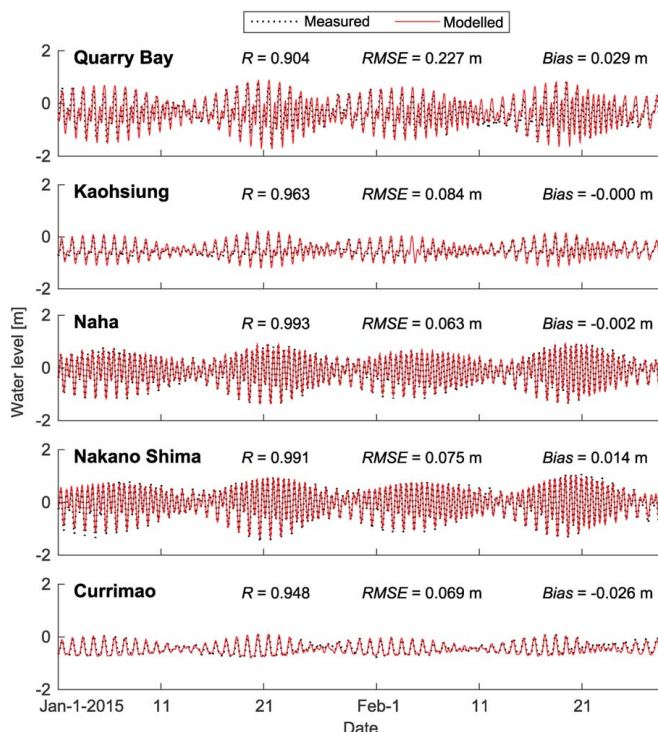


Fig. 4. (Color) Comparison of simulated and measured water levels, due to the astronomical tide, at selected tidal gauges (see Fig. 3 for gauge locations).

inaccuracies in the interpolated bathymetry owing to a relatively coarse grid resolution inside the Victoria Harbor.

Wind and Atmospheric Pressure Fields of Typhoon Maria

Several snapshots of the simulated wind and atmospheric pressure fields are shown in Fig. 5; these three selected instants are representative of (1) pre-landfall; (2) landfalling; and (3) post-landfall periods. Because of the interaction between the storm and the mountains on

Taiwan, the wind speed is reduced slightly and the wind field becomes asymmetric. However, the closest distance between Taiwan's coast and the eye of the passing typhoon is about 100 km, which is too large for the topography to significantly affect the typhoon's core structure. Numerical results from both scenarios are compared with the measurements at six selected meteorological gauge stations in Fig. 6. Overall, the model–data comparisons show that the WRF model was able to reasonably represent Maria's wind fields in terms of time series and the associated peak of wind speed at the stations near the best track. A good fit is also achieved at the Tainan station located in the far field of Maria's core, demonstrating WRF's strength in comprehensively reproducing the winds and pressures affected by other weather systems in addition to Typhoon Maria. By artificially lowering the hilly topography of Taiwan to 25% of its original values, the wind speeds and atmospheric pressures are minorly modified, but overall differences are not significant. However, wind speeds at Taiwan stations [Figs. 6(b and d)] show larger magnitudes around and after the peak hour, which are influenced by the decreased effect of island topography. At the same time, atmospheric pressures achieved lower values during the same period.

It is challenging for WRF to precisely simulate the storm track and the intensity at the same time. By defining the typhoon track center as the minimum atmospheric pressure, the simulated typhoon tracks from the WRF model are compared with the best track data obtained from CMA in Fig. 7. No significant differences in the simulated track locations are observed for the two WRF scenarios; however, the simulated tracks' locations are slightly southward of the best track data in the vicinity of Taiwan. Possibly due to the shift of the typhoon tracks in the WRF simulations, the wind speeds are overestimated at several meteorological stations [e.g., Figs. 6(c and e)]; the lowest pressure values are also slightly underestimated by WRF simulations as shown in Figs. 6(g–k). It is also noted that the simulated results have slight time lags (on the order of hours) in the movement of Typhoon Maria (Fig. 7). As the local wind stress at sea surface plays an important role in generating surges and waves, the overprediction in wind speeds and underestimation in pressures may lead to slightly overestimated surges and waves in coastal waters.

Storm Tides

The wind and pressure fields, generated for the two specific scenarios—the first scenario is hindcasting of Typhoon Maria; and the second scenario reduces the topographic heights in Taiwan to 25% of the original values, are used as drivers to produce storm-induced total water levels and wind waves. The total water level during the typhoon is defined as the sum of storm surge and astronomical tide and is also called storm tide. During Typhoon Maria, the temporal variations of storm tide have been recorded at tidal gauge stations on both sides of the Taiwan Strait and are compared with the simulated results in Fig. 8. The modeling suite is capable of resolving tidal fluctuations and reproducing storm tides at stations with different tidal ranges. The slight underestimations of storm tides along the Zhejiang coast are probably caused by the resolution of bathymetry data utilized in the present study. As shown in Fig. 6, the reduction of topographic heights in Taiwan does not change the wind and pressure fields significantly. Thus, it is not surprising to observe that the modification to Taiwan's topography does not change the resulting storm tides by any considerable amplitude (Fig. 8).

Significant Wave Height

The comparisons of simulated significant wave height with measurements at 10 buoy stations are shown in Fig. 9. The location

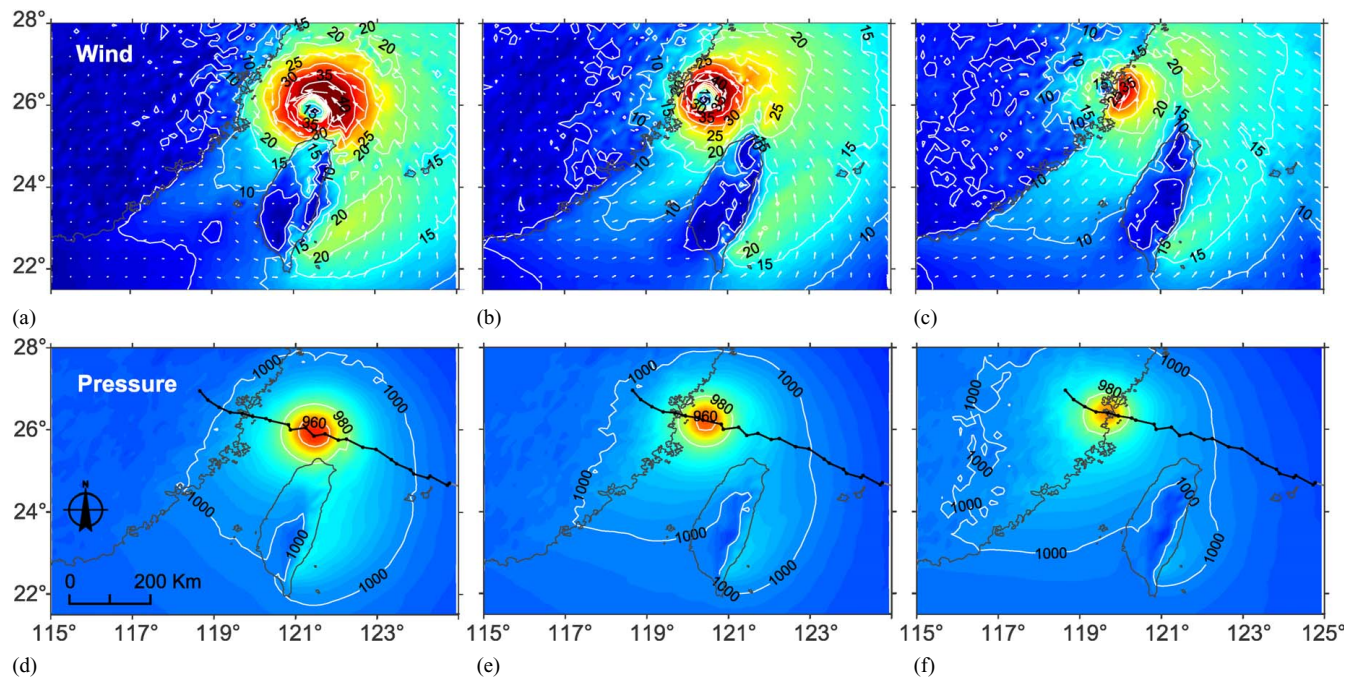


Fig. 5. (Color) Results of meteorological fields obtained from the WRF model at selected time instants: (a and d) 5:00 UTC+8 on July 11, 2018; (b and e) 9:00 UTC+8 on July 11, 2018; and (c and f) 12:00 UTC+8 on July 11, 2018. (a–c) Simulated 10-m height wind fields (unit: m/s); white contours indicate wind speed in 5 m/s increments; white arrows indicate wind directions; (d–e) simulated atmospheric pressure fields (unit: hPa); white contours indicate pressure in 20 hPa increments. (Shoreline data courtesy of GSHHG 2017.)

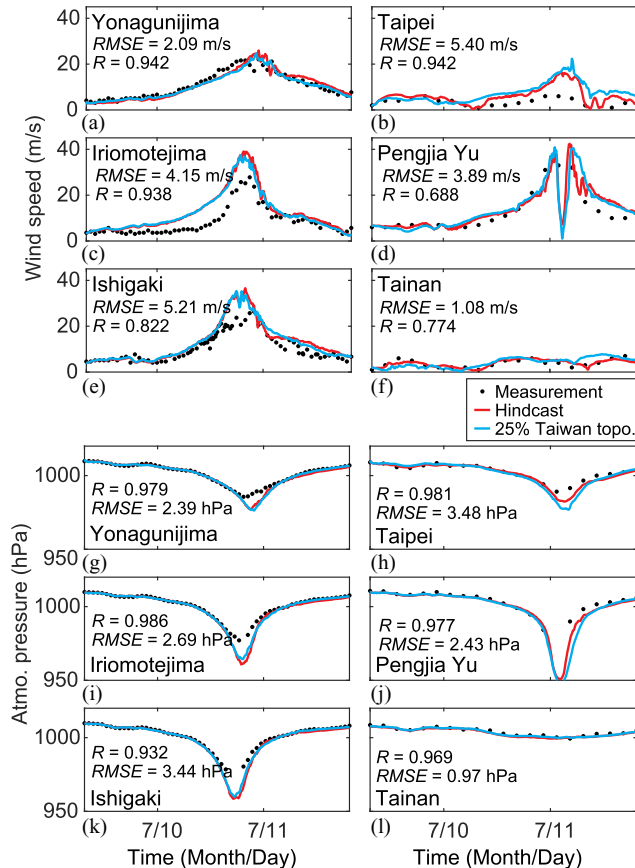


Fig. 6. (Color) Comparisons of numerical results of (a–f) 10-m height wind speeds; and (g–l) surface atmospheric pressures from WRF with measurements at selected locations (Fig. 3). Statistical metrics are assessed for the hindcast scenario (time zone: UTC+8).

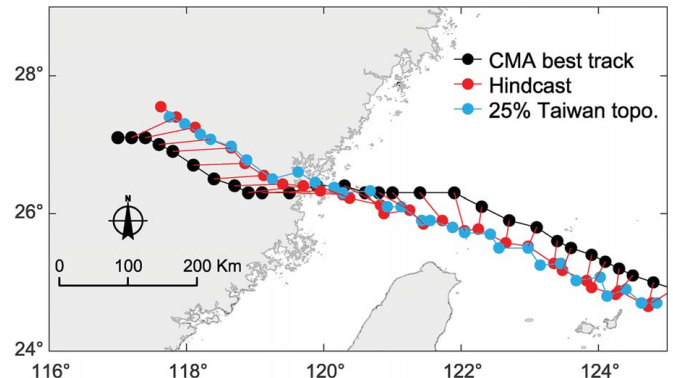


Fig. 7. (Color) Comparison of WRF simulated track locations (being defined as the minimum atmospheric pressure) with the best track data from CMA. Red lines connect cotemporal pairs of hindcast and CMA track centers.

of these buoy stations can be identified in Fig. 3. Overall, reasonable agreement has been achieved. The wave height peaks, ranging from 2.5 to 12 m at different stations, are adequately reproduced. We have also compared the mean wave periods at five stations around Taiwan Island (Fig. 3). It is again noted that modifying the topographic heights of Taiwan does not result in any large change in significant wave height. In addition, the model skill for reproducing the spatial variation of wave heights is examined by comparing the simulated significant wave height with the Ku-band significant wave height obtained from the Jason-3 altimeter data. During Cycle 089, the closest orbit to the typhoon eye was chosen for comparison (Fig. 10). The snapshot shown in Fig. 10 represents the field of significant wave height at 17:40 UTC+8 on July 11, 2018, for the hindcast scenario, which was 8.5 h after Typhoon Maria's landfall. Although

the effect of the storm on nearshore waters had diminished, a maximum wave height of approximately 5 m was still observed. The spatial distribution of measured wave heights along the satellite track was well reproduced by the simulation results.

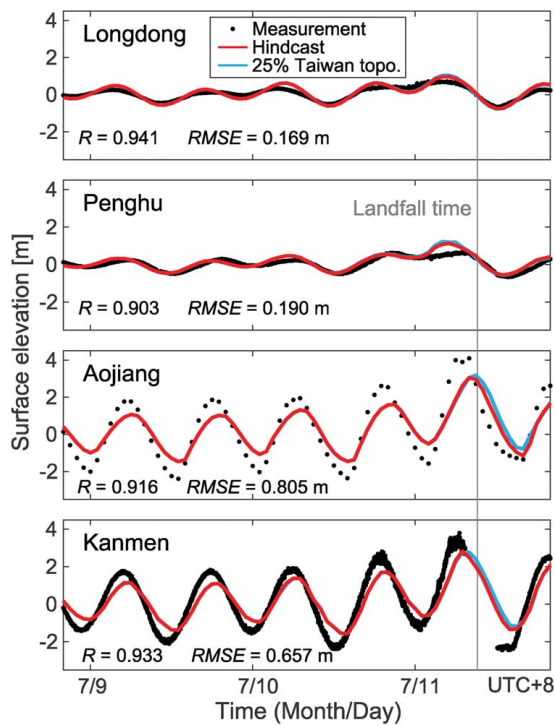


Fig. 8. (Color) Comparisons of simulated and measured storm tides at different tide gauges (Fig. 3). Statistical metrics are assessed for the hindcast scenario.

Additional Results and Discussions

Variation of Waves and Their Effects on Surge Heights

In Figs. 11(a–c), snapshots of simulated significant wave height at three instants (same as those shown in Fig. 5) are presented. Owing to the asymmetric pattern of the wind fields (Fig. 5), the significant wave height also distributes asymmetrically [Figs. 11(a–c)]. The high wave heights appear on the right-hand side of the typhoon track, which is obtained from the hindcast scenario of WRF model results by locating minimum atmospheric pressures. The wave heights can reach as high as 18 m on the continental shelf during the pre-landfall period. Moreover, significant wave height is larger in the northern ocean region of Taiwan than those in close proximity to the Zhejiang and Fujian coast, mainly because of the differences in energy dissipation associated with wave breaking and bottom friction. The results are consistent with measurements shown in Fig. 9. In Figs. 11(d–i), snapshots of storm tide and storm surge alone at the same three time instants are also displayed. According to Fig. 8, the snapshots in Figs. 11(a,d,g, and j) are during the pre-landfall period and show the distribution of storm tides in flood tide (Fig. 11d), while the other two snapshots Figs. 11(e and f) display the distributions during ebb tide. Owing to storm surge, waters are piled up along the coast of Fujian Province and in Taiwan Strait around the time of landfall, and the Taiwan Strait continues to experience elevated water levels for several hours after landfall (Figs. 11(g–i)).

To further investigate the effects of wind waves on storm surge, additional numerical simulations for storm tide with the Typhoon Maria conditions, but without including radiation stress, have been performed. In Figs. 11(j–l), the surge differences between simulation results with and without including the effects of wind waves are shown. The storm surge near the eye of Typhoon Maria is dominated by the low pressure system, and the effects of wind waves are insignificant

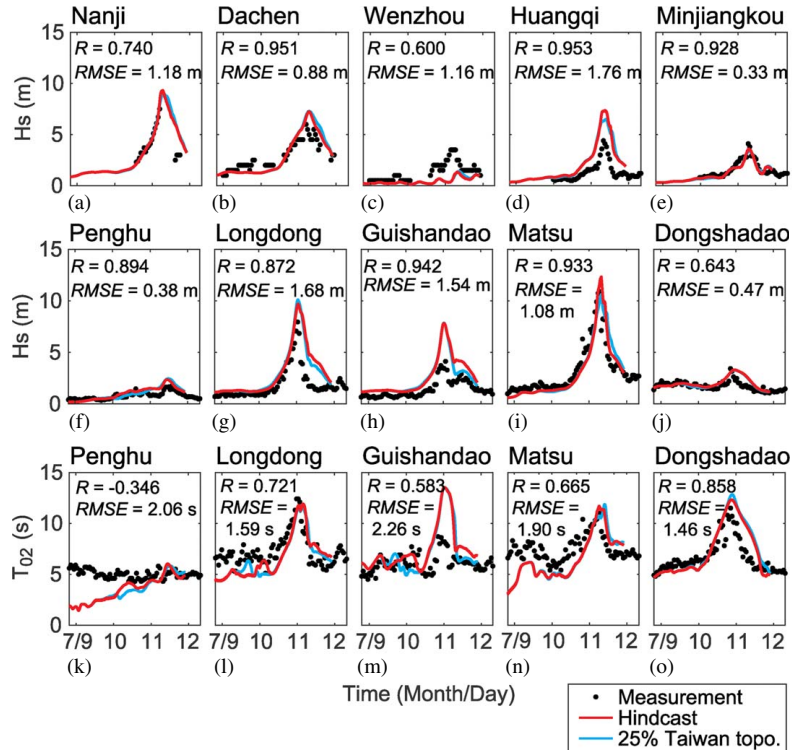


Fig. 9. (Color) Comparisons of (a–j) simulated and measured significant wave height; and (k–o) mean wave period at selected tide gauges (Fig. 3). Statistical metrics are assessed for the hindcast scenario (time zone: UTC+8).

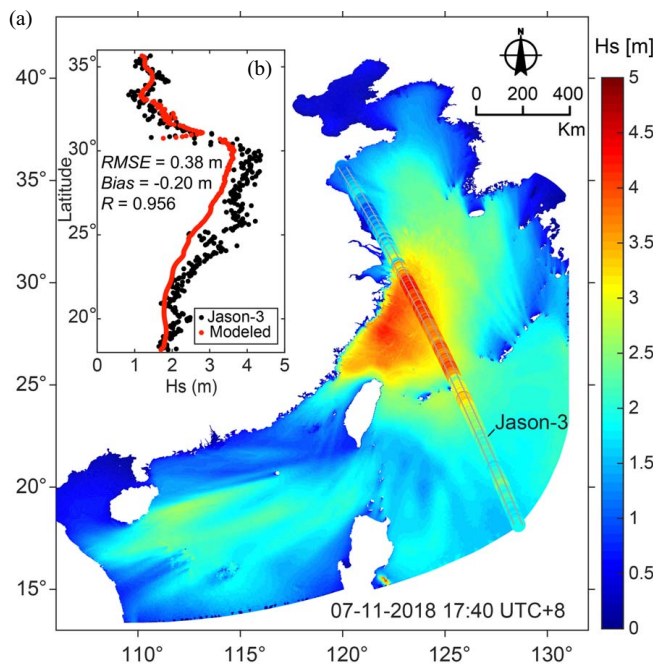


Fig. 10. (Color) (a) Simulated field of significant wave height (hindcast scenario) at 17:40 UTC+8 on July 11, 2018 and the Ku-band significant wave height observed from the Jason-3 altimeter data (Cycle 89, Track 62; overlaid with dots using the same color bar); and (b) the comparison of simulated significant wave height with altimeter data along the orbit.

[Figs. 11(g and j)]. Comparatively, the wind wave effects on surges in the nearshore areas are very noticeable, which are mainly influenced by the local wave set-up and set-down in shallow water [Fig. 11(k)]. The features of surges contributed by wind waves differ at different periods. Previous studies (Chen et al. 2019; Bertin et al. 2015; Yu et al. 2017) reported a similar phenomenon of wave set-up nearshore and set-down offshore during various storm events in coastal areas, which are related to modulated bottom stress due to the nonlinear interaction with complex geometry. It seems that the spatial differences of wave set-up/set-down influenced by geometry cannot fully explain the contribution of waves during this typhoon event. Our interpretation is that the wind directions of typhoon fields (Fig. 5) are possibly critical factors influencing wave set-up and set-down in different periods. The contribution of waves reaches maximum near the landfalling hour, as shown in Figs. 11(j-l).

The maximum values of simulated significant wave height and surge heights are plotted in Figs. 12(a and b). Maximum wave heights up to 18 m are generated on the continental shelf by the lasting strong winds as Typhoon Maria passes by the northern tip of Taiwan. In the shallow coastal waters, the significant wave height is reduced rapidly mainly because of wave breaking and bottom friction. Nevertheless, the maximum wave heights remain approximately 5 m in the vicinity of the landfall location. Being influenced by large waves, the maximum surge heights vary from about 0.2 m to nearly 3 m. Approximately 800 km of coastline experiences surge heights greater than 0.5 m during Typhoon Maria, and approximately 400 km of that coastline experiences surge heights greater than 1 m. The coastal area on the right-hand side of the typhoon landfall location experiences the largest surges. As shown in Fig. 12(b), the surge heights are influenced by Taiwan and larger surges occur in the Taiwan strait (on the west side of Taiwan), where they are 0.3–0.6 m higher than those in the east coast waters.

Through nonlinear effects (via radiation stress) wind waves indirectly affect generation and propagation of storm surge and become more significant in coastal waters. According to past studies, during certain storm events the maximum wind wave contribution to the peak surge level could reach 20%–40% in various areas, such as Tosa Bay, Japan, Gulf of Mexico, and Pearl River Estuary, China (Chen et al. 2019; Kim et al. 2010; Sheng et al. 2010). Here, we also examine the differences between the maximum storm surge heights with and without considering wind wave (radiation stress) effects [Figs. 12(c and d)]. Clearly, wind waves increase surge heights almost everywhere in the region, except in the vicinity of the right-hand side of the typhoon best track. Consequently, an average increment of 0.5 m (45%–60% of the hindcast scenario) and a decrement of 0.2 m (5%–21% of the hindcast scenario) are observed along the two sides of the best track of Typhoon Maria. The surge height differences reach their maximum in the nearshore areas along the Zhejiang and Fujian coasts mainly owing to the wave amplification effect.

Winds, Waves, and Surges Influenced by Island Topography

We plot the maximum wind speeds throughout the entire simulation for the hindcast and reduced topography scenarios, as well as the differences between them, in Fig. 13. In the hindcast simulation [Fig. 13(a)], the maximum wind speeds show more significant decay along the typhoon track since the typhoon circulation has been destroyed by terrain, and the width in the along-coast direction for wind speed larger than 40 m/s is about half of that from the reduced topography scenario [Fig. 13(b)]. The higher topography in the hindcast scenario [Fig. 13(a)] also causes higher typhoon winds (considerable areas with winds above 50 m/s occur to the northeast of Taiwan) than the reduced topography scenario [Fig. 13(b)]. From the perspective of meteorological dynamics, island topography plays an important role in not only blocking but also the formation of a channeling effect as a Pacific high pressure to the north of Typhoon Maria in this case. Therefore, the wind speed has been enhanced to the northeast of Taiwan in the hindcast simulation. Due to the height differences in the hindcast and the reduced topography scenarios, the typhoon circulation to the east of Taiwan nearly penetrates the mountains and thus, the wind flow [blue vector in Fig. 14(a)] is westerly in the latter scenario. However, the typhoon circulation cannot direct pass over the high mountains in the hindcast scenario. Instead, it goes around them [red vector in Fig. 14(a)], forming a strong southerly wind on the lee side of the mountains. The resulting differences in maximum wind speeds and spatial patterns are displayed in Fig. 13(c). In the reduced topography scenario, the wind speeds are generally larger in the Taiwan Strait and in the coastal waters along Fujian and Zhejiang Provinces due to the weakened blocking effect, but are smaller to the east of Taiwan due to the absence of the southerly wind. Finally, the channeling effect is quite weak so that the typhoon intensities during its lifetime remain steady in the reduced topography scenario [blue curve in Fig. 14(b)], while the typhoon circulation is seriously destroyed by the terrain leading to even weaker typhoon intensity in the hindcast scenario [red curve in Fig. 14(b)].

In Fig. 15, we show distribution of maximum wave heights and maximum storm surge from the results of the reduced topography scenario and the corresponding differences in maximum wave heights and maximum storm surge driven by the wind/pressure fields generated in the two WRF scenarios discussed previously. For the scenario that the mountain heights in Taiwan are reduced, the maximum significant wave height during Typhoon Maria tends to increase in waters around Taiwan [Fig. 15(c)]. On the continental shelf (north of

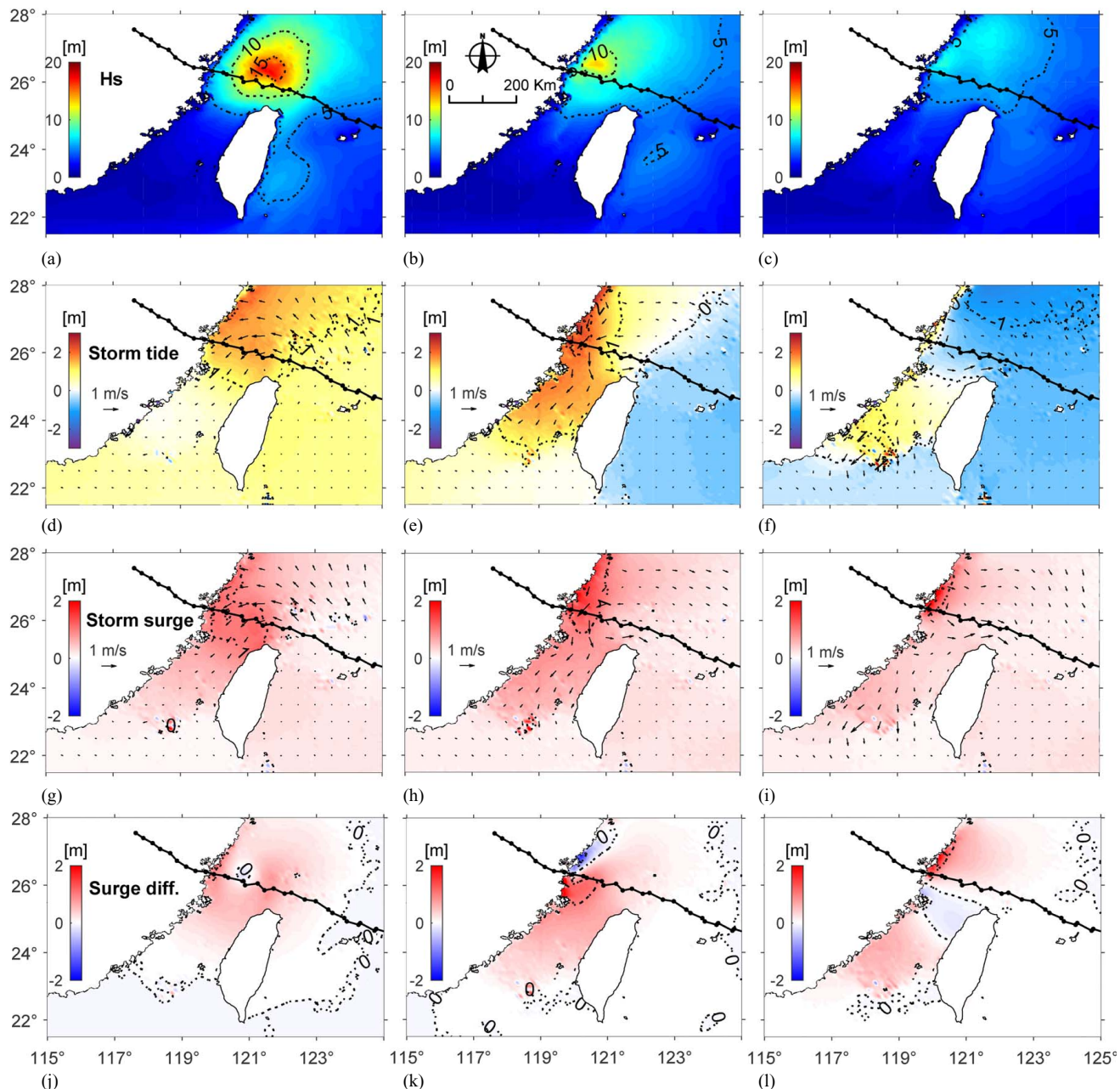


Fig. 11. (Color) Snapshots of simulation results at selected times: (a, d, g, and j) 5:00 UTC+8 on July 11, 2018; (b, e, h, and k) 9:00 UTC+8 on July 11, 2018; and (c, f, i, and l) 12:00 UTC+8 on July 11, 2018. The track location is derived from the WRF hindcast results, where the track center is defined by locating the minimum atmospheric pressure at each time step. (a–c) Significant wave height; (d–f) storm tide (storm surge plus astronomical tide); currents are shown using black arrows; (g–i) storm surge (including the effects of waves); currents are shown using black arrows; and (j–l) contribution to storm surge by waves (storm surge with radiation stress minus storm surge without radiation stress). (Shoreline data courtesy of GSHHG 2017.)

Taiwan) smaller wave heights are observed, which is probably attributed to the nonlinear processes being influenced by the wave–surge interaction. When the mountain heights in Taiwan are reduced, the storm surge along Fujian and Zhejiang Provinces is increased by 0.6–1.0 m on the right-hand side of typhoon track and decreased by 0.2–0.4 m on the opposite side. This variation reaches a percentage level of 64% to 110% and –20% to –40%, respectively, which is mainly caused by a northward landfall location (Fig. 7) in the reduced topography scenario. As shown in Fig. 12(b), the maximum of maximum (MOM) of surge height is located next to the right-hand side of the typhoon track. This location shifts northeastwardly in the reduced

topography scenario [Fig. 15(b)] and thus this shift of MOM location leads to the variation of the maximum storm surge in Fig. 15(d).

Effect of Surge on Currents

From the results presented in the “Variation of Waves and Their Effects on Surge Heights” section, it is clear that surge waves propagate mostly southwestwardly through Taiwan Strait (see surge evolution in Fig. 11). The topographic characteristics of Taiwan Island also contribute to increasing local surge heights during Typhoon Maria. We first investigate the variation of currents via Taiwan Strait by comparing the maximum hindcasted current velocities during the typhoon

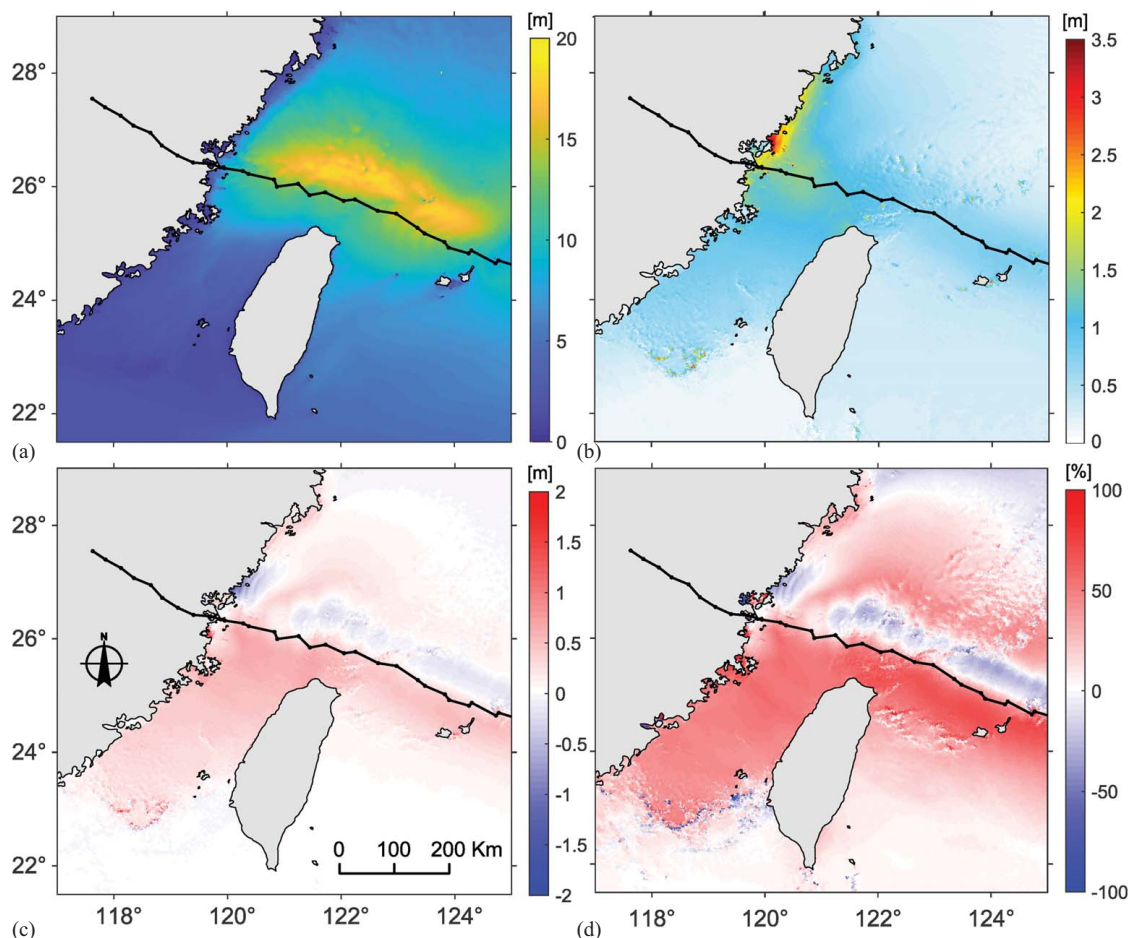


Fig. 12. (Color) (a) Maximum significant wave height values; (b) maximum storm surge values (including the effects of waves); (c) maximum contribution to storm surge by waves (*maximum storm surge with radiation stress minus maximum storm surge without radiation stress*); and (d) corresponding percentage level of wave-induced storm surge. The track location is derived from the WRF hindcast results, where the track center is defined by locating the minimum atmospheric pressure at each time step.

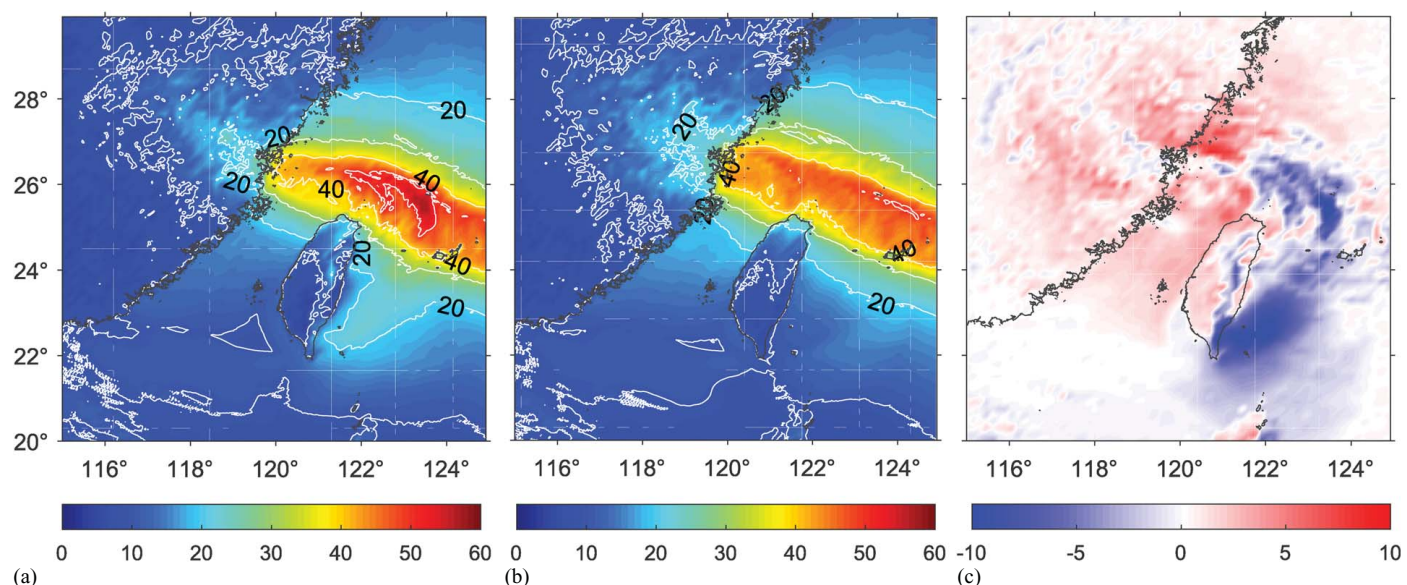


Fig. 13. (Color) Maximum wind speeds (unit: m/s) during the entire simulation for (a) hindcast scenario; (b) reduced topography scenario; and (c) the differences in maximum wind speeds due to island topography (*reduced topography scenario minus hindcast scenario*). (Shoreline data courtesy of GSHHG 2017.)

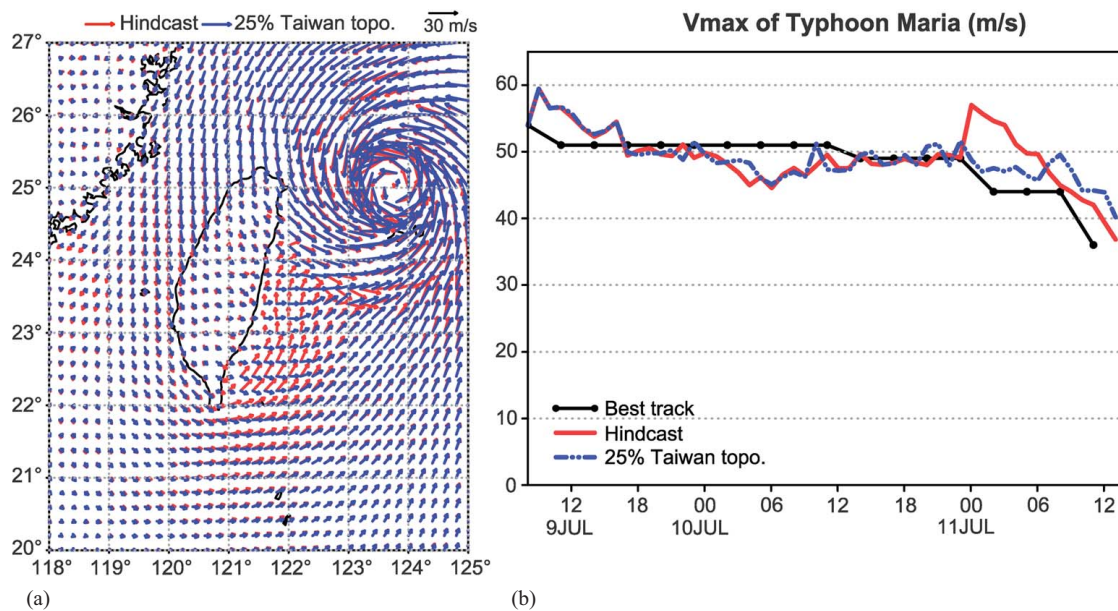


Fig. 14. (Color) (a) Wind vectors of Typhoon Maria on July 10, 2018 (21:00 UTC+8); and (b) time series of maximum wind speed (V_{\max}) in these two simulation scenarios (time zone: UTC+8).

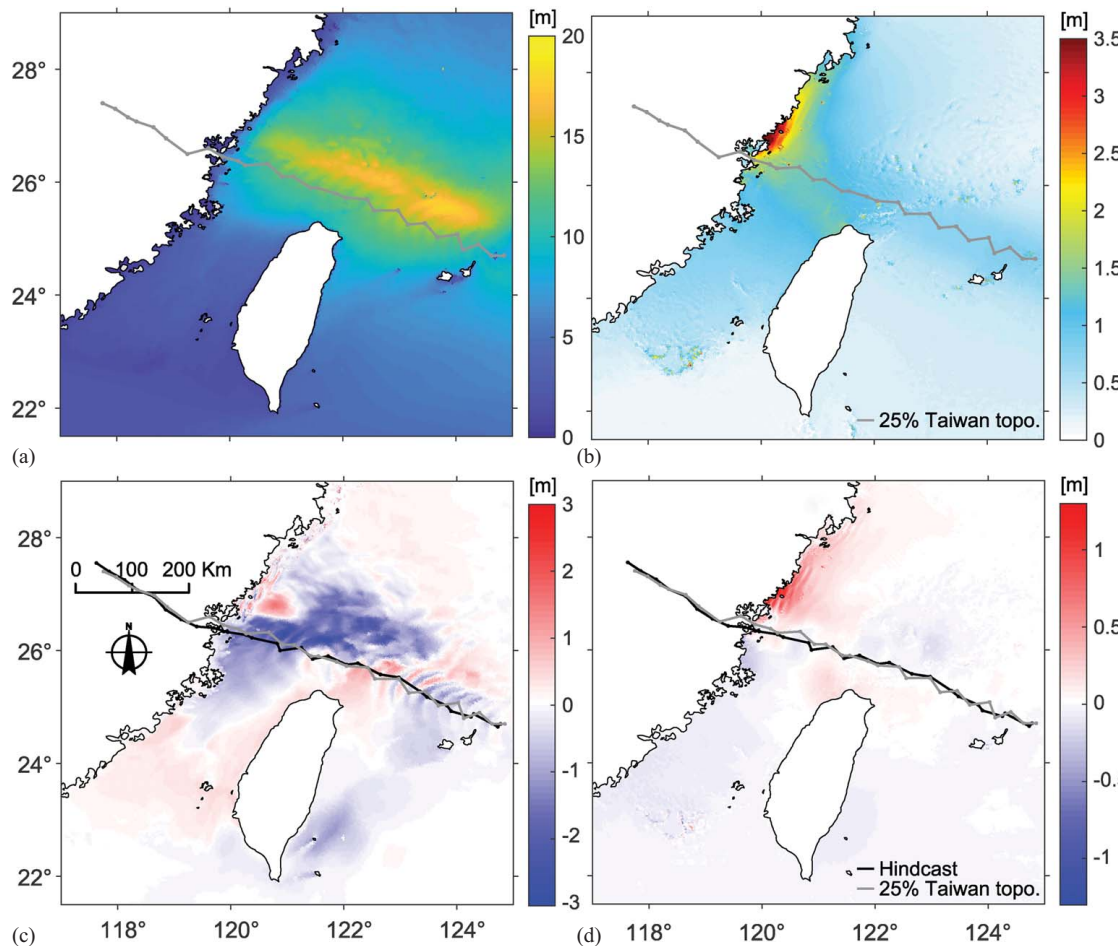


Fig. 15. (Color) (a) Maximum significant wave height from the reduced topography scenario; (b) maximum storm surge from the reduced topography scenario; (c) differences in maximum significant wave height; and (d) differences in maximum storm surge (reduced topography scenario minus hindcast scenario).

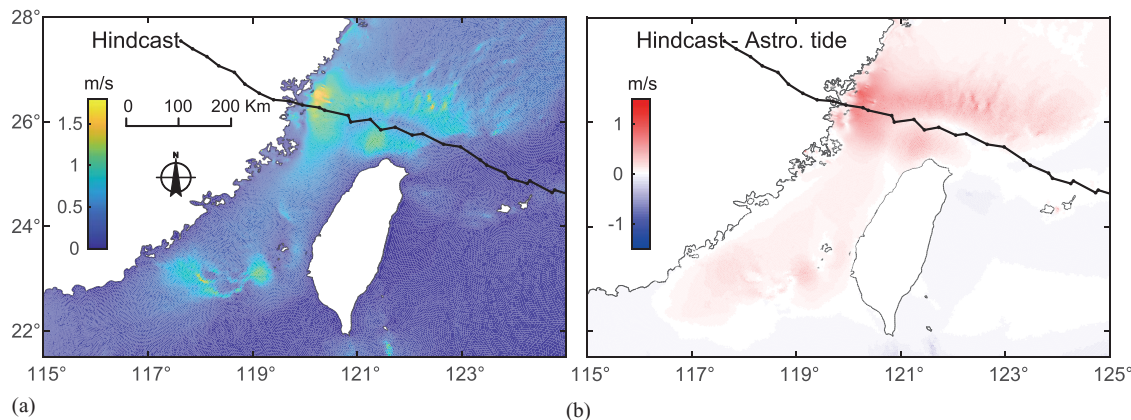


Fig. 16. (Color) (a) Maximum current velocities during Typhoon Maria; and (b) differences in maximum current velocities due to storm surge. The track location is derived from the WRF hindcast results, where the track center is defined by locating the minimum atmospheric pressure at each time step.

event [Fig. 16(a)] with the maximum current velocities associated with astronomical tide. In Fig. 16(b) the differences between those two are shown. It is clear that storm-induced currents are strongest along the typhoon track and in nearshore shallow waters.

To further illustrate the influences of storm surge in the Taiwan Strait, we exhibit a time sequence of current velocities across a cross section of Taiwan Strait during three scenarios in Fig. 17. The selected cross section is shown in Fig. 17(a). Three scenarios are presented in Fig. 17(b): (1) currents associated with astronomical tide (first column); (2) currents associated with the storm tide during Typhoon Maria (second column); and (3) currents associated with the storm tide in the reduced topography scenario during Typhoon Maria (third column). From the differences among these scenarios [fourth and fifth columns in Fig. 17(b)], it is clear that the currents induced during Typhoon Maria move mostly southwestwardly for at least 12 h before landfall. The current velocity reaches the maximum value of approximately 0.7 m/s in the hindcast scenario and is majorly contributed by storm-induced current along the Taiwan Strait [second and fourth columns in Fig. 17(b)]. In the reduced scenario, the storm-induced currents are slightly weakened by a maximum of about 0.1 m/s [fifth column in Fig. 17(b)]. This could be explained from the decrement of surge heights inside the Taiwan Strait shown in Fig. 15(d).

We also quantify the net volume fluxes across the Taiwan Strait for various scenarios during the Typhoon Maria event. A positive magnitude of volume flux indicates northeastwardly net transport [Fig. 18(a)]. In Fig. 18(a), the volume fluxes associated with storm tide are plotted, while the volume fluxes associated with the storm surge alone are shown in Fig. 18(b). It is clear that the effects of typhoon begin as early as about 48 h before Typhoon Maria's landfall. The volume fluxes due to the storm surge are in the southwestward direction before the landfall, which is consistent with the wind velocity field. After landfall, the direction of the volume fluxes reverses. This is indicated by the red and blue curves crossing the x -axis in Fig. 18(b). During these 48 h, the volume fluxes due to storm surge overwhelm those associated with tide so that the total volume fluxes due to storm tide are also in the southwestward direction [Fig. 18(a)]. Comparing the blue curve in Fig. 18(b) with the black curve in Fig. 18(a), the storm-induced southward flux is at a similar magnitude of that induced by the astronomical tide (variable depending on tidal timing). It indicates that the combined effects of the storm tide and the astronomical tide can increase flux magnitude up to an equivalent level as that induced by astronomical tide alone. Further investigation of the difference in net flux between the two topography scenarios shows that there

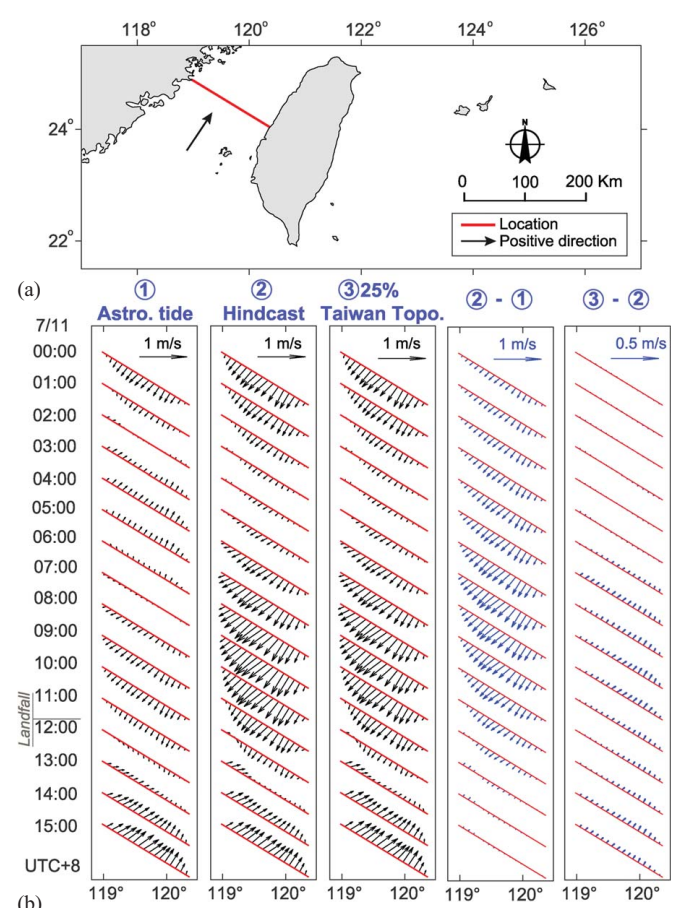


Fig. 17. (Color) (a) Location of the cross section for current velocity profile calculations in the Taiwan Strait; and (b) hourly velocity profiles during three scenarios (astronomical tide alone, hindcast simulation for Maria, and the reduced topography scenario for Maria) and the differences between scenarios (hindcast scenario minus tide-only scenario and reduced topography scenario minus hindcast scenario).

is a positive net flux (indicated by the black dashed line above the x -axis) beginning shortly before landfall in Fig. 18(b). This difference in flux can be attributed to the difference in island topography; there is less flux in the southwestward direction in the case of the reduced topography. This is to be expected given the reduced surge in the Taiwan Strait in the reduced topography scenario

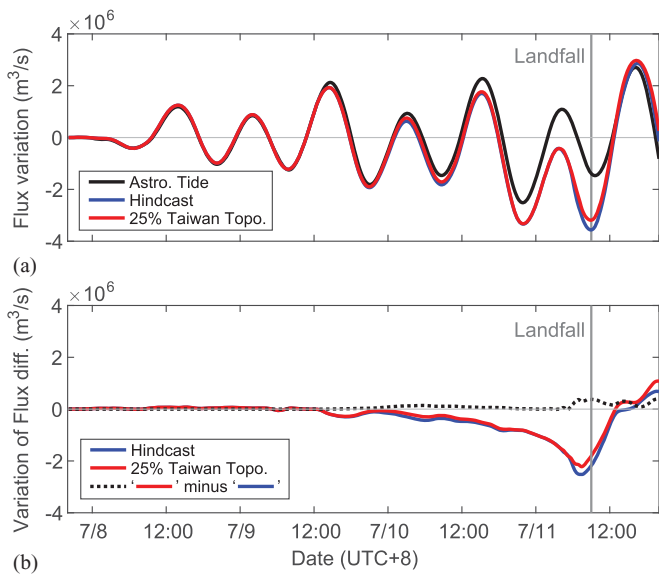


Fig. 18. (Color) (a) Time series of volume flux through Taiwan Strait during Typhoon Maria; and (b) the net flux variation owing to storm surge and difference due to reduced island topography.

[Fig. 15(d)]. This maximum difference of flux is approximately 16% compared with the maximum flux from the hindcast simulation results, which indicates that the barrier effect of the island is related to the island topographical height, and the reduced topography of island decreased storm-induced flux in the Taiwan Strait by about 16%.

Conclusions

Typhoon Maria was one of the most damaging storm events in the western North Pacific in 2018, which caused extraordinary hazards in Taiwan, Zhejiang, and Fujian. Typhoon Maria avoided a direct hit of Taiwan but still was influenced by the mountainous topography of Taiwan Island. The mountainous topography causes partial decay of storm winds, and it also influences surge wave propagation and surge heights around the Taiwan waters. In this study, we execute a hindcast simulation of this representative typhoon event to examine associated patterns of surges and waves in this region using a wind–surge–wave modeling suite. The model suite consists of a WRF model for calculating meteorological conditions at the sea surface and a circulation model, SCHISM, coupled with a spectral wave module, WWMIII, for computing tides, surges and waves. The data–model comparison suggests that the skill of this modeling suite is high and reliable for reproducing key features of this event. Surface winds, water levels, and waves associated with the typhoon are well reproduced along the Fujian and Zhejiang coasts, as well as in waters around Taiwan. It is notable that the WRF model can successfully forecast both storm track and intensity with high resolution, and it can resolve the asymmetric wind fields impacted by local mountainous topography, which are shown to be crucial for accurate storm surge simulation. Compared with parametric vortex models, which generate wind and atmospheric pressure fields based on best track data, it is more challenging for climate models such as WRF to accurately predict typhoon track and intensity at the same. As simulation results show in this study, the predicted track of Maria is slightly southwardly shifted, although key structures and movements of this storm have been reproduced. This shift is possibly the main reason in

slight overestimation of wind speed and wind wave heights at stations on the northern Taiwan coast.

The storm-induced wave heights are closely related to surface wind stress and distribute asymmetrically at different instants during Typhoon Maria. The higher wave heights occur on the right-hand side as the anticlockwise movement of rotational winds agrees with typhoon forward direction there. The processes of storm tide and surge height indicate that storm-induced waters are piled up along the coast of Fujian Province and in Taiwan Strait around the landfalling hour, and the Taiwan Strait continues to experience elevated water levels for several hours after landfall owing to storm surge. Influenced by local wave set-up and set-down in shallow waters, the effects of waves on surge heights can be clearly observed, especially in the nearshore areas. The maximum significant wave height over the continental shelf during Typhoon Maria was up to approximately 18 m but decreased rapidly to a magnitude of approximately 5 m near the landfalling coast due to wave breaking and bottom friction. The distribution of maximum storm surges indicates that the coasts along northern Taiwan, Fujian, and Zhejiang suffered storm damages at different levels. Approximately 400 km of coastline experienced surge heights larger than 1 m, in which Fujian and Zhejiang are the most severely affected coasts being exposed to intensive surge. The surge height near northern Taiwan is significantly smaller than near the Fujian and Zhejiang coasts, although large wave heights were induced when Maria passed by. The presence of Taiwan Island altered the surge wave propagation prior to landfall and slightly elevated the surge heights inside the Taiwan Strait by 0.3–0.6 m.

With the assistance of the tightly coupled surge–wave model SCHISM, we conducted additional numerical experiments to better understand the role of waves in affecting surge patterns and heights. When the surge wave propagates from deep ocean to the continental shelf, the wave-induced surge begins to account for a larger proportion of the overall surge height. The effects of waves, via radiation stress, causes an average increment of 0.5 m and a decrement of 0.2 m on the left-hand and right-hand sides of the moving typhoon track, respectively. This accounts for an increase in surge of 45%–60% and a decrease in surge of 5%–21%, on the left-hand and right-hand sides of the track, respectively.

Investigation has also been conducted on the effects of topography change on winds, and accordingly on waves and storm surges, which illustrate the variation of their patterns being influenced by the nonlinear interaction between surge and waves. Due to the terrain-induced blocking effect, the results show that the high topography leads to more significant decay of winds and smaller width of areas with wind speed larger than 40 m/s along coast than the reduced topography scenario. Moreover, the higher island topography of the hindcast scenario intensifies wind speed to the northeast of the Taiwan Island due to the channeling effect. The differences in wind patterns caused by reducing the heights of the island topography further lead to the increment of maximum significant wave height in waters around Taiwan. At the same time, the reduced topography scenario also leads to elevated surge heights by 0.6–1.0 m on the right-hand side of typhoon landfalling coasts but smaller surge (by 0.2–0.4 m) in the Taiwan Strait. The storm-induced currents in Taiwan Strait are further investigated. Storm surge tends to increase the southwestwardly flux via the Taiwan Strait with larger current velocities, and the combined effect of storm surge and astronomical tide increases flux magnitude up to an equivalent level as that induced by astronomical tide alone. Compared with the storm-induced current, the maximum variation of current velocity due to different topography heights is as small as approximately 0.1 m/s.

The findings of the present study improve our understanding of how island topography influences typhoons and thus influences

dynamic storm surge processes. It demonstrates how the wind field, storm surge, and waves are altered by the presence of an island, as well as the importance of the nonlinear surge–wave interaction. The modeling suite utilized in the present study can be applied to other storm studies.

Data Availability Statement

Numerical models and some data used during the study were provided by a third party. Direct requests for these materials may be made to the provider as indicated in the Acknowledgements.

Acknowledgments

We would like to dedicate this paper to Professor Theodore Yaotsu Wu of Caltech for his leadership in water wave research and its applications to coastal hazards. This research was supported by the National Key Research and Development Program of China (Grant No. 2018YFC0407506) and the Ng Teng Fong Charitable Foundation (Hong Kong) under the joint research project “The impact of climate changes on coastal flooding hazard in South and East China Seas” between National University of Singapore and Tsinghua University. This work was also supported by the Key Laboratory of Ministry of Education for Coastal Disaster and Protection in Hohai University, Guangdong Province Introduced Innovative R&D Team of Geological Processes and Natural Disasters around the South China Sea (2016ZT06N331), and National Natural Science Foundation of China (41774049, 41976197 and 51761135015). The WRF model can be downloaded from <https://www2.mmm.ucar.edu/wrf/users/downloads.html> after registration. The SCHISM modeling suite is available at <http://ccrm.vims.edu/schismweb>. The meteorological data for comparing WRF results was obtained from <https://gis.ncdc.noaa.gov/maps/ncei>, and the astronomical tide data was retrieved from <https://uhslc.soest.hawaii.edu/>. The GEBCO data used in this study was downloaded from <http://www.gebco.net> in October 2014. The navigational charts in the Zhejiang and Fujian Provinces were purchased from Beijing Situo Ocean Information Technology Co. Ltd. The coastline data used for establishing numerical model and generating plots was retrieved from the GSHHG (Global Self-consistent, Hierarchical, High-resolution Geography Database) shoreline database (Wessel and Smith 1996; <https://www.ngdc.noaa.gov/mgg/shorelines/gshhs.html>). The hindcast products of WAVEWATCHIII were downloaded from <ftp://ftp.ifremer.fr/ifremer/ww3/HINDCAST>.

References

- Bertin, X., K. Li, A. Roland, and J.-R. Bidlot. 2015. “The contribution of short-waves in storm surges: Two case studies in the Bay of Biscay.” *Cont. Shelf Res.* 96: 1–15. <https://doi.org/10.1016/j.csr.2015.01.005>.
- Booij, N., R. C. Ris, and L. H. Holthuijsen. 1999. “A third-generation wave model for coastal regions: 1. Model description and validation.” *J. Geophys. Res.* 104 (C4): 7649–7666. <https://doi.org/10.1029/98JC02622>.
- Chambers, C., and T. Li. 2011. “The effect of Hawai’i’s Big Island on track and structure of tropical cyclones passing to the south and west.” *Mon. Weather Rev.* 139 (11): 3609–3627. <https://doi.org/10.1175/MWR-D-11-00031.1>.
- Chen, C., et al. 2013. “Extratropical storm inundation testbed: Intermodel comparisons in Scituate, Massachusetts.” *J. Geophys. Res.: Oceans* 118 (10): 5054–5073. <https://doi.org/10.1002/jgrc.20397>.
- Chen, Y., L. Chen, H. Zhang, and W. Gong. 2019. “Effects of wave-current interaction on the Pearl River estuary during Typhoon Hato.” *Estuarine Coastal Shelf Sci.* 228: 106364. <https://doi.org/10.1016/j.ecss.2019.106364>.
- Chen, C., H. Liu, and R. C. Beardsley. 2003. “An unstructured grid, finite-volume, three-dimensional, primitive equations ocean model: Application to coastal ocean and estuaries.” *J. Atmos. Oceanic Technol.* 20: 159–186. [https://doi.org/10.1175/1520-0426\(2003\)020<0159:AUGFVT>2.0.CO;2](https://doi.org/10.1175/1520-0426(2003)020<0159:AUGFVT>2.0.CO;2).
- CMA. 2008. “Weather China.” Weather Service Center of CMA. Accessed July 11, 2018. <http://typhoon.weather.com.cn/>.
- Egbert, G. D., and S. Y. Erofeeva. 2002. “Efficient inverse modeling of barotropic ocean tides.” *J. Atmos. Oceanic Technol.* 19 (2): 183–204. [https://doi.org/10.1175/1520-0426\(2002\)019<0183:EIMBO>2.0.CO;2](https://doi.org/10.1175/1520-0426(2002)019<0183:EIMBO>2.0.CO;2).
- Emanuel, K., and R. Rotunno. 2011. “Self-stratification of tropical cyclone outflow. Part I: Implications for storm structure.” *J. Atmos. Sci.* 68 (10): 2236–2249. <https://doi.org/10.1175/JAS-D-10-05024.1>.
- Fang, X., Y. Kuo, and A. Wang. 2011. “The impacts of Taiwan topography on the predictability of Typhoon Morakot’s record-breaking rainfall: A high-resolution ensemble simulation.” *Weather Forecasting* 26 (5): 613–633. <https://doi.org/10.1175/WAF-D-10-05020.1>.
- Fortunato, A. B., P. Freire, X. Bertin, M. Rodrigues, J. Ferreira, and M. L. R. Liberato. 2017. “A numerical study of the February 15, 1941 storm in the Tagus estuary.” *Cont. Shelf Res.* 144: 50–64. <https://doi.org/10.1016/j.csr.2017.06.023>.
- Grell, G. A., J. Dudhia, and D. R. Stauffer. 1994. *A description of the fifth-generation Penn State/NCAR mesoscale model (MM5)*. NCAR Tech. Note NCAR/TN-392STR. Boulder, CO: National Center for Atmospheric Research.
- Holland, G. J. 1980. “An analytic model of the wind and pressure profiles in hurricanes.” *Mon. Weather Rev.* 108 (8): 1212–1218. [https://doi.org/10.1175/1520-0493\(1980\)108<1212:AAMOTW>2.0.CO;2](https://doi.org/10.1175/1520-0493(1980)108<1212:AAMOTW>2.0.CO;2).
- Hong, S.-Y., J. Dudhia, and S.-H. Chen. 2004. “A revised approach to ice microphysical processes for the bulk parameterization of clouds and precipitation.” *Mon. Weather Rev.* 132 (1): 103–120. [https://doi.org/10.1175/1520-0493\(2004\)132<0103:ARATIM>2.0.CO;2](https://doi.org/10.1175/1520-0493(2004)132<0103:ARATIM>2.0.CO;2).
- Hong, S.-Y., Y. Noh, and J. Dudhia. 2006. “A new vertical diffusion package with an explicit treatment of entrainment processes.” *Mon. Weather Rev.* 134 (9): 2318–2341. <https://doi.org/10.1175/MWR3199.1>.
- Hsu, T.-W., S.-H. Ou, and J.-M. Liau. 2005. “Hindcasting nearshore wind waves using a FEM code for SWAN.” *Coastal Eng.* 52 (2): 177–195. <https://doi.org/10.1016/j.coastaleng.2004.11.005>.
- Huang, Y.-H., C.-C. Wu, and Y. Wang. 2011. “The influence of island topography on typhoon track deflection.” *Mon. Weather Rev.* 139 (6): 1708–1727. <https://doi.org/10.1175/2011MWR3560.1>.
- Iacono, M. J., J. S. Delamere, E. J. Mlawer, M. W. Shephard, S. A. Clough, and W. D. Collins. 2008. “Radiative forcing by long-lived greenhouse gases: Calculations with the AER radiative transfer models.” *J. Geophys. Res.* 113 (D13): D13103. <https://doi.org/10.1029/2008JD009944>.
- Jian, G., and C. Wu. 2008. “A numerical study of the track deflection of Supertyphoon Haitang (2005) prior to its landfall in Taiwan.” *Mon. Weather Rev.* 136 (2): 598–615. <https://doi.org/10.1175/2007MWR2134.1>.
- Jiménez, P. A., J. Dudhia, J. F. González-Rouco, J. Navarro, J. P. Montávez, and E. García-Bustamante. 2012. “A revised scheme for the WRF surface layer formulation.” *Mon. Weather Rev.* 140 (3): 898–918. <https://doi.org/10.1175/MWR-D-11-00056.1>.
- Kain, J. S. 2004. “The Kain–Fritsch convective parameterization: An update.” *J. Appl. Meteorol.* 43 (1): 170–181. [https://doi.org/10.1175/1520-0450\(2004\)043<0170:TKCPAU>2.0.CO;2](https://doi.org/10.1175/1520-0450(2004)043<0170:TKCPAU>2.0.CO;2).
- Kain, J. S., and J. M. Fritsch. 1990. “A one-dimensional entraining/detraining plume model and its application in convective parameterization.” *J. Atmos. Sci.* 47 (23): 2784–2802. [https://doi.org/10.1175/1520-0469\(1990\)047<2784:AODEPM>2.0.CO;2](https://doi.org/10.1175/1520-0469(1990)047<2784:AODEPM>2.0.CO;2).
- Kim, S. Y., T. Yasuda, and H. Mase. 2010. “Wave set-up in the storm surge along open coasts during Typhoon Anita.” *Coastal Eng.* 57 (7): 631–642. <https://doi.org/10.1016/j.coastaleng.2010.02.004>.
- Krien, Y., et al. 2017. “Towards improved storm surge models in the northern Bay of Bengal.” *Cont. Shelf Res.* 135: 58–73. <https://doi.org/10.1016/j.csr.2017.01.014>.
- Li, L., et al. 2018. “Field survey of Typhoon Hato (2017) and a comparison with storm surge modeling in Macau.” *Nat. Hazards Earth Syst. Sci.* 18: 3167–3178. <https://doi.org/10.5194/nhess-18-3167-2018>.

- Liu, W.-C., and W.-C. Huang. 2020. "Investigating typhoon-induced storm surge and waves in the coast of Taiwan using an integrally-coupled tide-surge-wave model." *Ocean Eng.* 212: 107571. <https://doi.org/10.1016/j.oceaneng.2020.107571>.
- Liu, Z., H. Wang, Y. J. Zhang, L. Magnusson, J. D. Loftis, and D. Forrest. 2020. "Cross-scale modeling of storm surge, tide, and inundation in Mid-Atlantic Bight and New York City during Hurricane Sandy, 2012." *Estuarine Coastal Shelf Sci.* 233: 106544. <https://doi.org/10.1016/j.ecss.2019.106544>.
- Luettich, R. A., J. J. Westerink, and N. W. Scheffner. 1992. *ADCIRC: An advanced threedimensional circulation model for shelves, coasts and estuaries*. Report 1: Theory and methodology of ADCIRC-2DDI and ADCIRC-3DL, Dredging Research Program Technical Report DRP-92-6. Vicksburg, MS: US Army Engineers Waterways Experiment Station.
- Ma, L.-M., and Z.-M. Tan. 2009. "Improving the behavior of the cumulus parameterization for tropical cyclone prediction: Convection trigger." *Atmos. Res.* 92 (2): 190–211. <https://doi.org/10.1016/j.atmosres.2008.09.022>.
- National Environmental Satellite Data and Information Service. 2018. "Jason-3: Gathering environmental intelligence from the world's oceans." Accessed July 28, 2018. <https://www.nesdis.noaa.gov/jason-3/>.
- Pond, S., and G. L. Pickard. 1983. *Introductory dynamical oceanography*. 2nd ed. Oxford: Butterworth-Heinemann.
- Roland, A., A. Cucco, C. Ferrarin, T.-W. Hsu, J.-M. Liau, S.-H. Ou, G. Umgiesser, and U. Zanke. 2009. "On the development and verification of a 2-D coupled wave-current model on unstructured meshes." *J. Mar. Syst.* 78: S244–S254. <https://doi.org/10.1016/j.jmarsys.2009.01.026>.
- Sheng, Y. P., Y. Zhang, and V. A. Paramygin. 2010. "Simulation of storm surge, wave, and coastal inundation in the Northeastern Gulf of Mexico region during Hurricane Ivan in 2004." *Ocean Modell.* 35 (4): 314–331. <https://doi.org/10.1016/j.ocemod.2010.09.004>.
- Skamarock, W. C., J. B. Klemp, J. Dudhia, D. O. Gill, D. Barker, M. G. Duda, X.-y. Huang, W. Wang, and J. G. Powers. 2008. *A description of the advanced research WRF version 3*. NCAR Technical Note. Boulder, CO: National Center for Atmospheric Research.
- Tang, C. K., and J. C. L. Chan. 2014. "Idealized simulations of the effect of Taiwan and Philippines topographies on tropical cyclone tracks." *Q. J. R. Meteorolog. Soc.* 140 (682): 1578–1589. <https://doi.org/10.1002/qj.2240>.
- Tang, C. K., and J. C. L. Chan. 2015. "Idealized simulations of the effect of local and remote topographies on tropical cyclone tracks." *Q. J. R. Meteorolog. Soc.* 141 (691): 2045–2056. <https://doi.org/10.1002/qj.2498>.
- Tang, C. K., and J. C. L. Chan. 2016a. "Idealized simulations of the effect of Taiwan topography on the tracks of tropical cyclones with different sizes." *Q. J. R. Meteorolog. Soc.* 142 (695): 793–804. <https://doi.org/10.1002/qj.2681>.
- Tang, C. K., and J. C. L. Chan. 2016b. "Idealized simulations of the effect of Taiwan topography on the tracks of tropical cyclones with different steering flow strengths." *Q. J. R. Meteorolog. Soc.* 142 (701): 3211–3221. <https://doi.org/10.1002/qj.2902>.
- Tewari, M., F. Chen, W. Wang, J. Dudhia, M. A. LeMone, K. Mitchell, M. Ek, G. Gayno, J. Wegiel, and R. H. Cuenca. 2004. "Implementation and verification of the unified Noah land surface model in the WRF model." In *Proc., 20th Conf. on Weather Analysis and Forecasting/16th Conf. on Numerical Weather Prediction*. Seattle, WA: American Meteorological Society.
- Tolman, H. L., J.-H. G. Alves, and Y. Y. Chao. 2005. "Operational forecasting of wind-generated waves by hurricane Isabel at NCEP." *Weather Forecasting* 20 (4): 544–557. <https://doi.org/10.1175/WAF852.1>.
- Tolman, H. L., B. Balasubramanyan, L. D. Burroughs, D. V. Chalikov, Y. Y. Chao, H. S. Chen, and V. M. Gerald. 2002. "Development and implementation of wind-generated ocean surface wave models at NCEP." *Weather Forecasting* 17 (2): 311–333. [https://doi.org/10.1175/1520-0434\(2002\)017<0311:DAIOWG>2.0.CO;2](https://doi.org/10.1175/1520-0434(2002)017<0311:DAIOWG>2.0.CO;2).
- Vickery, P. J., D. Wadhera, M. D. Powell, and Y. Chen. 2009. "A hurricane boundary layer and wind field model for use in engineering applications." *J. Appl. Meteorol. Climatol.* 48 (2): 381–405. <https://doi.org/10.1175/2008JAMC1841.1>.
- Wang, C., Y. Chen, H. Kuo, and S. Huang. 2013. "Sensitivity of typhoon track to asymmetric latent heating/rainfall induced by Taiwan topography: A numerical study of Typhoon Fanapi (2010)." *J. Geophys. Res. D: Atmos.* 118 (8): 3292–3308. <https://doi.org/10.1002/jgrd.50351>.
- Wessel, P., and W. H. F. Smith. 1996. "A global self-consistent, hierarchical, high-resolution shoreline database." *J. Geophys. Res. Solid Earth* 101: 8741–8743. <https://doi.org/10.1029/96JB00104>.
- Wu, C.-C. 2001. "Numerical simulation of Typhoon Gladys (1994) and its interaction with Taiwan terrain using the GFDL hurricane model." *Mon. Weather Rev.* 129 (6): 1533. [https://doi.org/10.1175/1520-0493\(2001\)129<1533:NSOTGA>2.0.CO;2](https://doi.org/10.1175/1520-0493(2001)129<1533:NSOTGA>2.0.CO;2).
- Xie, B., and F. Zhang. 2012. "Impacts of typhoon track and Island topography on the heavy rainfalls in Taiwan associated with Morakot (2009)." *Mon. Weather Rev.* 140 (10): 3379–3394. <https://doi.org/10.1175/MWR-D-11-00240.1>.
- Xie, L., S. Bao, L. J. Pietrafesa, K. Foley, and M. Fuentes. 2006. "A real-time hurricane surface wind forecasting model: Formulation and verification." *Mon. Weather Rev.* 134 (5): 1355–1370. <https://doi.org/10.1175/MWR3126.1>.
- Xue, L., and Y. Li. 2016. "The effect of mesoscale systems induced by the topography of Taiwan on the rapid intensification of typhoon Meranti (1010)." [In Chinese.] *Chin. J. Atmos. Sci.* 40 (6): 1107–1116.
- Yang, J., et al. 2019. "A comparative study of Typhoon Hato (2017) and Typhoon Mangkhut (2018)—Their impacts on coastal inundation in Macau." *J. Geophys. Res.: Oceans* 124 (12): 9590–9619. <https://doi.org/10.1029/2019JC015249>.
- Yang, M., D. Zhang, X. Tang, and Y. Zhang. 2011. "A modeling study of Typhoon Nari (2001) at landfall: 2. Structural changes and terrain-induced asymmetries." *J. Geophys. Res.: Atmos.* 116 (D9): D09112. <https://doi.org/10.1029/2010JD015445>.
- Yang, M.-J., D.-L. Zhang, and H.-L. Huang. 2008. "A modeling study of Typhoon Nari (2001) at landfall. Part I: Topographic effects." *J. Atmos. Sci.* 65 (10): 3095–3115. <https://doi.org/10.1175/2008JAS2453.1>.
- Yeh, T.-C., and R. L. Elsberry. 1993. "Interaction of typhoons with the Taiwan orography. Part I: Upstream track deflections." *Mon. Weather Rev.* 121 (12): 3193–3212. [https://doi.org/10.1175/1520-0493\(1993\)121<3193:IOTWTT>2.0.CO;2](https://doi.org/10.1175/1520-0493(1993)121<3193:IOTWTT>2.0.CO;2).
- Yu, X., W. Pan, X. Zheng, S. Zhou, and X. Tao. 2017. "Effects of wave-current interaction on storm surge in the Taiwan Strait: Insights from Typhoon Morakot." *Cont. Shelf Res.* 146: 47–57. <https://doi.org/10.1016/j.csr.2017.08.009>.
- Zhang, W.-Z., H.-S. Hong, S.-P. Shang, X.-H. Yan, and F. Chai. 2009. "Strong southward transport events due to typhoons in the Taiwan Strait." *J. Geophys. Res.* 114: C11013. <https://doi.org/10.1029/2009JC005372>.
- Zhang, W.-Z., F. Shi, H.-S. Hong, S.-P. Shang, and J. T. Kirby. 2010. "Tide–surge interaction intensified by the Taiwan Strait." *J. Geophys. Res.* 115: C06012. <https://doi.org/10.1029/2009JC005762>.
- Zhang, Y., and A. M. Baptista. 2008. "SELFE: A semi-implicit Eulerian–Lagrangian finite-element model for cross-scale ocean circulation." *Ocean Modell.* 21 (3–4): 71–96. <https://doi.org/10.1016/j.ocemod.2007.11.005>.
- Zhang, Y. J., F. Ye, E. V. Stanev, and S. Grashorn. 2016. "Seamless cross-scale modeling with SCHISM." *Ocean Modell.* 102: 64–81. <https://doi.org/10.1016/j.ocemod.2016.05.002>.